Electrochimica Acta 449 (2023) 142176

Contents lists available at ScienceDirect

Electrochimica Acta

journal homepage: www.journals.elsevier.com/electrochimica-acta

Exploring the use of oligomeric carbonates as porogens and ion-conductors in phase-separated structural electrolytes for Lithium-ion batteries

Samuel Emilsson [a], Vidyanand Vijayakumar [b], Jonas Mindemark [b], Mats Johansson [a,*]

[a] Department of Fibre & Polymer Technology, KTH Royal Institute of Technology, Stockholm, Sweden
[b] Department of Chemistry – Ångström Laboratory, Uppsala University, Uppsala, Sweden

ARTICLE INFO

Keywords:
Structural batteries
Polymer electrolyte
Polymerization-induced phase separation
Ionic conductivity
McMullin number
Carbonate oligomers
Lithium ion

ABSTRACT

Phase-separated structural battery electrolytes (SBEs) have the potential to enhance the mechanical stability of the electrolyte while maintaining a high ion conduction. This can be achieved via polymerization-induced phase separation (PIPS), which creates a two-phase system with a liquid electrolyte percolating a mesoporous thermoset. While previous studies have used commercially available liquid electrolytes, this study investigates the use of novel oligomeric carbonates to enhanced the safety of the SBEs. Increasing the carbonate chain length significantly enhances the thermal stability of the SBEs. Tuning the molecular structure of the liquid electrolyte has a significant effect on the PIPS process and SBE morphology. Using a combination of analyses on a series of wet and dried SBEs, the complex interplay between the phases is interpreted. When an increased pore size is achieved, it leads to a lower MacMullin number (N_M). A conductivity of 2×10^{-5} S/cm with a N_M=13 could be achieved, while maintaining a thermal stability up to 150 °C. The present study demonstrates a versatile approach to tailor this type of electrolyte.

1. Introduction

The need for batteries is growing due to the transformation away from fossil fuels. According to the IPCC's recent report on climate change mitigation, employment of electromobility through batteries plays a vital role in reaching the climate goals [1]. For this, lighter and more energy-dense batteries are needed; by far, lithium-ion batteries are the current state-of-the-art technology. These conventional batteries employ liquid electrolytes based on a combination of cyclic and linear carbonate solvents owing to their high ionic conductivity. However, the linear carbonates are sensitive to higher temperatures due to their volatility and decreasing electrochemical stability as the temperature is increased [2]. Furthermore, employing new battery technologies such as Li-metal electrodes and structural batteries put requirements on the electrolyte which presently used liquid electrolytes cannot solely fulfil [3,4].

Replacing intercalation graphite-based anodes with Li-metal anodes has the potential to enhance the energy density of Li-ion batteries significantly [5]. However, due to the reactivity of the Li-metal surface, dendrites tend to form during the lithium plating process, leading to an increase in overpotential and acceleration of electrolyte decomposition. Dendrite growth can also lead to short circuits as they pierce through the separator. To hinder this, two main strategies have been pursued. The first strategy involves controlling the plating process to avoid the nucleation of dendrites. Examples include modifying the copper current collector or adding pulses of high current densities to ensure more nucleation sites for Li deposition [5,6].

The second strategy involves developing solid-state electrolytes which can hinder dendrites from growing thanks to their mechanical robustness. Potentially, a higher electrochemical stability can also be achieved. For this, solid polymer electrolytes are an alternative to conventional inorganic solid-state electrolytes. However, high molecular weights in polymer electrolytes often lead to low room temperature ionic conductivity. The conductivity is significantly enhanced by raising the temperature, but this often leads to poor mechanical properties that accommodate dendrite growth [7]. A trade-off between mechanical integrity and conductivity thus exists for most homogeneous polymers. For example, efforts to improve the mechanical integrity include increasing the crosslinking density [8] or using block co-polymers with a stiff block at the expense of reduced ion conductivity [9].

The combination of high mechanical rigidity and uncompromised ion conduction is vital for developing electrolytes for structural battery

* Corresponding author.
E-mail address: matskg@kth.se (M. Johansson).

https://doi.org/10.1016/j.electacta.2023.142176
Received 19 December 2022; Received in revised form 13 February 2023; Accepted 4 March 2023
Available online 5 March 2023

composites. Structural batteries can use carbon fibres as the anode material owing to their ability to intercalate lithium ions, while also working as a reinforcing material and electrical conductor [10]. On the positive side, the carbon fibres can be coated with cathode material, acting as current collectors. Surrounding the electrode material, a polymer matrix is required to both transfer mechanical load and conduct lithium ions. Thus, the polymer matrix must exhibit a combination of high ionic conductivity and high stiffness [3,11].

To accommodate these requirements, structural battery electrolytes (SBEs) using a two-phase system separated on the sub-micron scale has shown promise. A mobile phase for ion conduction interpenetrates a porous thermoset with a high modulus that can transfer mechanical load [12].

Such SBEs can be synthesized using a process called polymerization-induced phase separation (PIPS) which combine solvents (the porogen) and monomer(s) with crosslinking capabilities which can be cured using heat or UV in the presence of an initiator. As the polymer grows during curing, it starts to become insoluble in the solvents, leading to phase separation [13]. Depending on the reaction conditions and formulations used, a wide variety of morphologies can be developed [14,15]. Some factors which can be used to tune the morphology includes: the porogen polarity and molecular weight [16,17], monomer choice [18,19], curing conditions [20,21], and formulation [20]. For this, the use of Hansen solubility parameters has become a powerful tool as a predictor for the PIPS capabilities of different formulations. PIPS can be found in the literature for a wide variety of applications, with column materials for chromatography accounting for a large portion of the research [22].

In the past decade, PIPS has also been utilized to form phase-separated electrolytes for energy storage of various types. Lodge et al. used phase-separating co-polymers containing a styrene/divinylbenzene block and a polyethylene glycol (PEG) block [23,24]. Shirshova et al. used ionic liquids in combination with an epoxy resin to obtain structural supercapacitor electrolytes [25,26]. This has been further developed by Choi et al. [27,28]. Several researchers have used oligomeric PEG as a porogen in epoxy resins [29,30]. Recently, Manly et al. also used PIPS to obtain thin battery separators in a one-step process [31].

In our group, Ihrner et al. used a liquid electrolyte based on ethylene carbonate (EC) and dimethyl methylphosphonate (DMMP), combined with dimethacrylate monomers to obtain SBEs with high modulus and ionic conductivity [32]. Further development of a thermally-initiated system allowed for their use in structural battery full cells [33,34]. Although these SBEs perform well at room temperature, they still employ traditional electrolyte solvents with their inherent limitations in terms of volatility and leakage. In addition, previous studies have mainly focused on varying the monomers and curing conditions, and less systematically on how the molecular structure of the liquid electrolytes affects the overall PIPS process and final performance.

Branched oligomeric carbonates have previously been synthesised for light-emitting electrochemical cells [35], and their structural similarity to dimethyl carbonate (DMC) and diethyl carbonate (DEC) makes them an interesting alternative in lithium-ion batteries. Polymeric carbonates, e.g. poly(trimethylene carbonate), also exhibit significantly higher Li transference number than PEG, although with a significantly lower total ion conductivity [36].

In the present study linear oligomeric carbonates were synthesised to act as porogens and oligomeric carbonate electrolyte. Thereby, the gap between using a liquid containing SBE and a two-phase polymer blend is explored. The effect of varying the chain length of the oligomeric carbonates on the phase separation and SBE end-performance is systematically investigated. This study shows that increasing the oligomer chain length significantly improves the thermal stability of the SBEs. Increasing the oligomer chain length also changes the phase separation, leading to the formation of larger pores. This leads to a lower McMullin number in the SBE, which can enhance the ionic conductivity. This study also acts as guide to developing novel SBEs, showing the complex interactions of parameters as different porogens are used.

2. Experimental

2.1. Materials

Bisphenol A ethoxylate dimethacrylate (Mn= 540 g/mol) was supplied by Sartomer Company, Europe. Trimethylene carbonate (TMC) was purchased from TCI Europe. 1,8-Diazabicyclo[5.4.0]undec-7-ene (DBU) (98%), 1,3-propanediol (98%), 2-dimethylaminoethanol (>99.5%), ethyl chloroformate, 2′.2′-azobis(2-methylpropionitrile) (AIBN) (98%), dichloromethane (DCM), dimethyl carbonate (DMC), and lithium bis(trifluoromethanesulfonyl)imide (LiTFSI) (99.99%) was purchased from Sigma Aldrich/Merck. Pyridine (99.9%) was purchased from VWR.

2.2. Oligomer synthesis

In inert conditions, a dried glass bottle was charged with 3 g of TMC and 1,3-propanediol (2.1 mL for O2, 0.7 mL for O4) was added at different amounts to control the DP. 45 μL DBU was added to catalyse the ring-opening reaction of TMC, and the glass bottle was sealed and heated to 60 °C on a heating plate under stirring. The reaction was left to proceed for 3 h. This resulted in a linear carbonate oligomer with hydroxyl end groups. In a second step, the oligomers were end-capped. The oligomer was subsequently dissolved in 80 mL DCM and transferred to a round-bottom flask cooled with an ice bath. Ethyl chloroformate (6.2 mL for O2, 2.06 mL for O4) was added dropwise to the solution under stirring, followed by pyridine (10.43 mL for O2, 3.48 mL for O4) which was added dropwise during 10 min. The reaction was then allowed to react overnight. The day after, the reaction was quenched with (2.94 mL for O2, 0.98 mL for O4) 2-dimethylaminoethanol. The end-capped oligomers were extracted using 80 mL deionized water, 2 × 80 mL 1 M HCl, and 80 mL saturated aqueous $NaHCO_3$. The organic phase was collected, dried with $MgSO_4$, and filtered. The solvent was evaporated in a rotary evaporator and the oligomer was dried for 72 h in a vacuum oven at 50 °C to remove any remaining solvent or water. ^{1}H NMR was used to confirm that the correct DP and end-capping were achieved and that the all solvent was removed (see S1).

O1 (a carbonate dimer) was synthesised by simply using the end-capping procedure described above, but with 1,3-propanediol as a reactant instead of an oligomer. 3 g 1,3-propanediol and 80 mL DCM were added to a round-bottom flask cooled in an ice bath. 8.29 mL ethyl chloroformate was added dropwise followed by 13.98 mL pyridine. The reaction was left overnight and 3.95 mL 2-dimethylaminoethanol was added to quench the reaction. The extraction was done in the same way as mentioned above, and the solvent was removed using a rotary evaporator. Typically, the last solvent residue was removed by drying in a vacuum oven for a few hours. The removal of solvent was confirmed with ^{1}H NMR. The dimer was dried using activated molecular sieves which were left for at least 24 h. Upon removal of the molecular sieves, the solution was filtered through a syringe filter with 0.1 μm pores.

2.3. SBE film preparation

Inside an argon-filled glovebox (<2 ppm O_2, <2 ppm H_2O) 20 wt% LiTFSI was dissolved in the dried oligomers. Subsequently, bisphenol A ethoxylate dimethacrylate was combined with the oligomeric electrolytes at fixed ratios in vials (40 or 50 wt% electrolyte). For O2 and O4, the mixtures were heated to ~ 50 °C to lower the viscosity and mixed with a vortex mixer. Once a homogeneous mixture was achieved, the mixture was cooled for a minute and AIBN (1 wt% of monomer) was added. The mixture was then vortexed again. Bubbles were removed by placing under vacuum in the glovebox antechamber. The mixture was then added to aluminium moulds using a syringe and a glass slide was place on top. Clamps were added to keep the glass slide in place. For DMA, FTIR, SEM and gas adsorption measurements, films were made using moulds for rectangular films (30 × 5 × 0.5 mm^3). For conductivity

measurements and cell fabrication, moulds for 15 mm discs (100 μm thick) were used. The moulds were sealed in pouch bags and brought outside the glovebox to cure in a preheated oven at 90 °C for 1 hour. Circular SBE films were removed from the moulds, with a thickness of around 100 μm.

For DMA, SEM, and gas adsorption measurements of the dried films, the films were first subjected to a solvent exchange in DMC for one week due to the high viscosity of the oligomers. Subsequently, the films were dried at 50 °C under vacuum for an additional week. The mass loss of the dried films was recorded.

2.4. Viscosity measurements

A TQC Sheen cone and plate viscometer was used for measuring the viscosity of the oligomeric carbonate electrolytes. Two cones (0–10 P; 10–100 P) were used to match the viscosity range of the liquid electrolytes.

2.5. Differential scanning calorimetry (DSC)

A DSC1 from Mettler Toledo with a sample robot was used. Around 10 mg of electrolyte was loaded into an aluminium pan. The samples were heated to 80 °C at 10 °C/min and subsequently cooled to −100 °C at 5 °C/min and finally heated to 80 °C at 5 °C/min. The glass transition temperature (T_g) was determined on the second heating as the midpoint of the slope change.

2.6. Fourier-transform infrared spectroscopy (FTIR)

A PerkinElmer Spectrum 100 was used in attenuated total reflection (ATR) mode equipped with a MKII Golden Gate ATR accessory (Specac Ltd.). Spectra of the resin mixture before curing and of the SBE films after curing were recorded. 16 spectra were collected at 4000–600 cm^{-1} at a resolution of 4 cm^{-1}. The conversion was calculated by comparing the area of the vinyl stretching peak of the methacrylate monomer at 1637 cm^{-1}. Spectra were normalized to the maximum height of the peak corresponding to the carbonyl, at around 1730 cm^{-1}.

2.5. Dynamic mechanical analysis (DMA)

A DMA Q800 from TA instruments in tension film mode, equipped with a liquid nitrogen cooling accessory was used to analyse the thermomechanical properties of the SBEs. The films were attached to the clamps at a 10–15 mm distance and subjected to 125% preload force, followed by 0.1% amplitude strain at a fixed frequency (1 Hz). The films were initially cooled to −100 °C and equilibrated for 10 min. The sample was heated to 200 °C at a 3 °C/min heating rate. The T_g of the oligomer and polymer was determined by the temperature at the tan δ peaks. Storage modulus and T_g values that are presented are an average of two runs.

2.6. Scanning electron microscopy (SEM)

A Hitachi S-4800 with a cold emission electron gun was used to investigate the morphology of the dried SBE films. The dried films were fractured by first dipping them in liquid nitrogen and then creating a cold fracture by bending them with tweezers. The films were attached to a cross-section 90° pin stub with the fractured surface exposed. A Cressington 208HR with a Pt/Pd target was used to sputter a 2 nm layer of Pt/Pd on the surface.

2.7. Nitrogen gas sorption

A BET 3 flex from Micromeritics was used to measure the gas adsorption of the dried films. The films were broken in half and loaded into 12 mm sample tubes. The samples were degassed for 1 hour at 60 °C followed by up to 3 days at 90 °C. The adsorption and desorption isotherms were obtained at the temperature of liquid nitrogen (77.3 K). The Brunauer–Emmett–Teller (BET) surface area was extracted from the adsorption isotherm at P/P_0=0.05–0.3. The average pore width was estimated from the desorption isotherm by Barrett-Joyner-Halenda (BJH) analysis using the Faas correction.

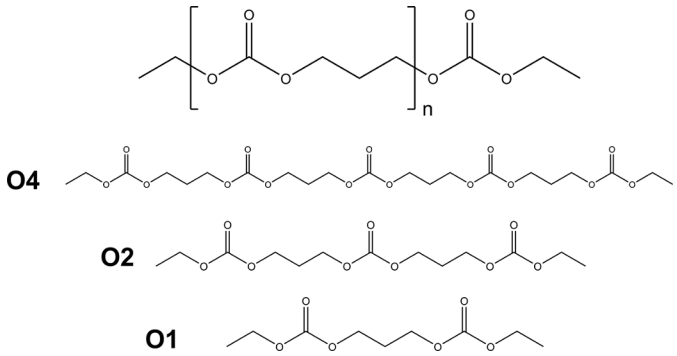

Fig. 1. Chemical structure of the synthesized oligomers. The top structure displays the general structure of the oligomers.

2.8. Electrochemical Impedance Spectroscopy (EIS)

The total ionic conductivity of the SBEs and oligomeric carbonate electrolytes were determined by electrochemical impedance spectroscopy (EIS) run between 1 Hz and 10 MHz with an amplitude of 10 mV. A Schlumberger SI 1260 Impedance/ Gain-phase analyzer was used.

Thin SBE discs were prepared in a mould as described above. The film (15 mm diameter, 100 μm thick) was sandwiched between two stainless steel blocking electrodes (15 mm diameter) in CR2032 coin cells. Each side was wetted by an additional 2 μl of the respective oligomeric carbonate electrolyte. This was done to counteract any evaporation or removal of the oligomers that may have occurred during preparation which would increase interfacial resistance. The cells were left to rest at 60 °C for 2 h prior to measurements. A Swagelok-type cell was used for the pure oligomeric carbonate electrolytes, using a Teflon spacer to control the distance between two blocking electrodes. The measurements were then carried out at an interval of 10 °C from room temperature to 60 °C. Duplicates of each formulation were made. The SBE and liquid ionic conductivities were found by fitting EIS data using RelaxIS 3.

3. Results and discussion

3.1. Synthesis of porous films

In this study, bisphenol A ethoxylate dimethacrylate was used as the monomer. It has previously shown to have ideal properties for SBEs since it is a relatively low-viscosity resin which when cured creates a stiff network with aromatic groups and high crosslink density. The porogen was varied by using linear carbonates of different lengths. Three linear carbonates were synthesized. These contained an average of 1, 2 and 4 (O1, O2, and O4) repeating units based on the structure in Fig. 1. The oligomers were end-capped with ethyl chloroformate to ensure less reactive end groups and ensure better miscibility with the monomer. After synthesis and purification, their structures were confirmed with

Table 1
Physical properties of synthesized oligomers combined with LiTFSI.

	η [Pa,s]	σ [S/cm]	T_g [°C]
O4 + 20 wt% LiTFSI	8.08	$2.6 \bullet 10^{-6}$	−48
O2 + 20 wt% LiTFSI	0.39	$2.6 \bullet 10^{-5}$	−71
O1 + 20 wt% LiTFSI	0.05	$2.4 \bullet 10^{-4}$	−91

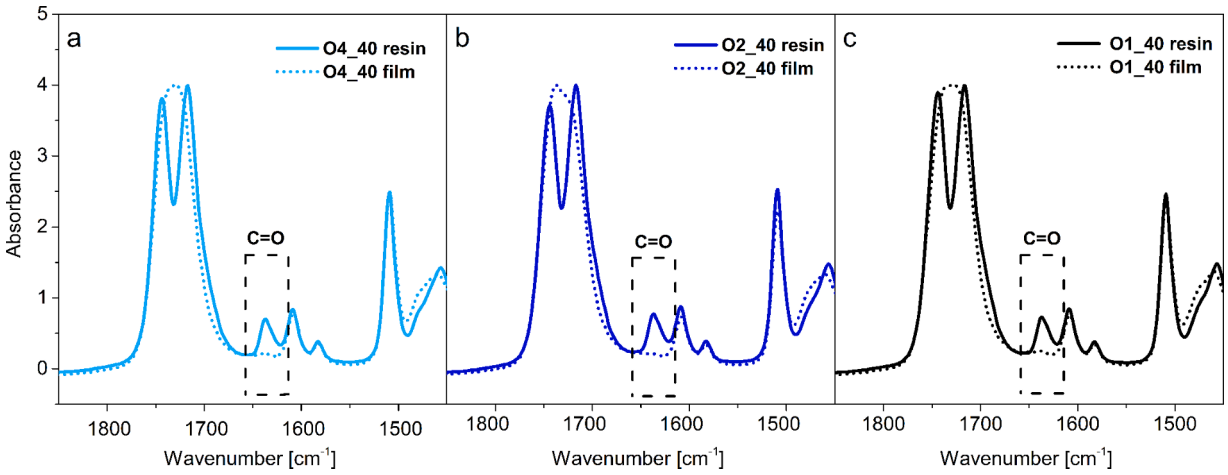

Fig. 2. FTIR spectra of a) O4_40 b) O2_40 and c) O1_40 before and after curing. The boxed region represents the vinyl stretching peak at 1637 cm^{-1}.

Table 2
Physical properties of SBE films before and after drying.

Sample	Conversion[a] (%)	Mass loss[b]	Volumetric shrinkage [%]	BET surface area [m^2/g]	Average pore size [nm][c]
O4_40	>95	39.7	17 ± 3	49.2	16.8
O2_40	>95	40.5	25 ± 3	46.6	9.8
O1_40	>95	40.5	36 ± 1	–	–
O1_50	91	50.1	27 ± 4	63.6	14.3

[a] Based on decrease in vinyl peak area in FTIR. The resolution limits finding conversions above 95% [b]After solvent exchange and drying. [c]Based on the BJH model on the desorption isotherm.

NMR (Fig. S2). Lithium bis(trifluoromethanesulfonyl)imide (LiTFSI) was dissolved at a fixed ratio (20 wt%) to obtain three different oligomeric carbonate electrolytes.

The properties of the oligomeric electrolytes can be seen in Table 1. Although structurally similar, the viscosity and conductivity change drastically. With increasing chain length, the viscosity increases with an order of magnitude and the ionic conductivity decreases with an order of magnitude. These properties will have a significant effect on both the phase separation process during curing, and subsequent properties of the obtained SBEs.

All three electrolytes were deemed miscible with the monomer. The more viscous O2 and O4 needed to be heated to properly mix with the monomer, but when cooled remained miscible. The Hansen solubility parameters for all oligomers were calculated using Hansen solubility parameters in practice (HSPiP), found in Table S2. Their solubility

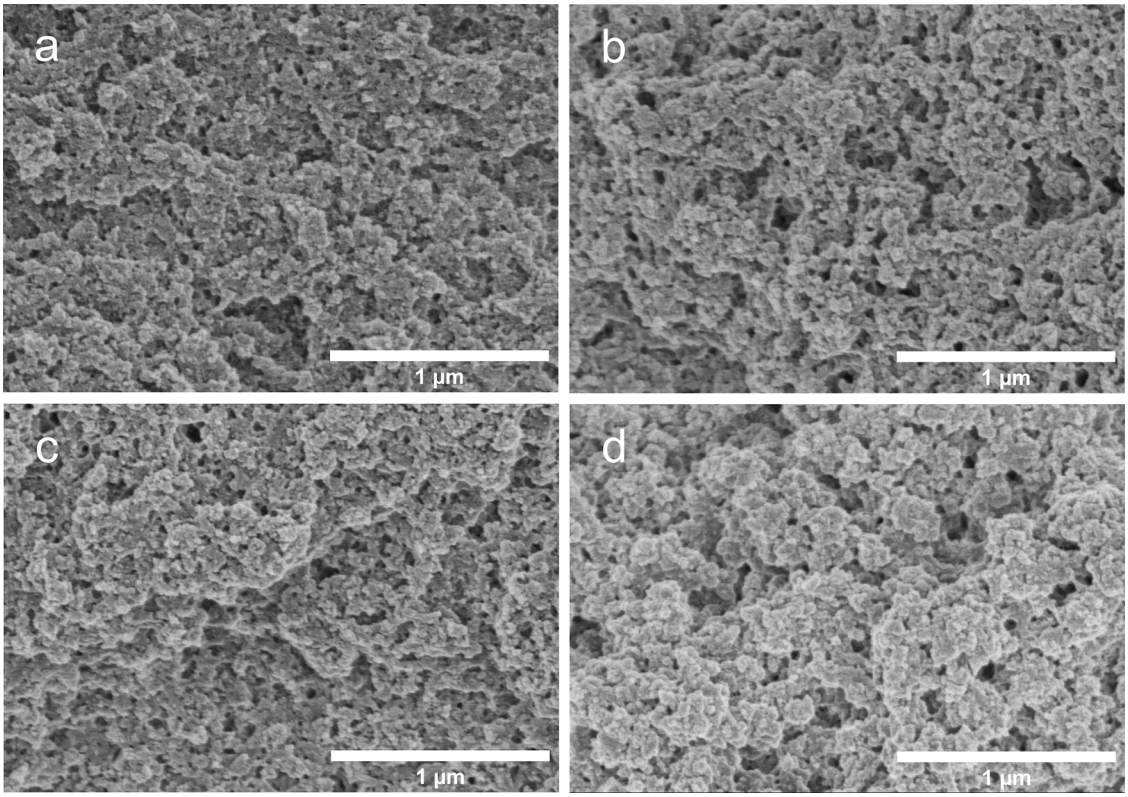

Fig. 3. FE-SEM micrographs of the cross-section of a) O1_40%, b) O1_50%, c) O2_40%, and d) O4_40% after drying.

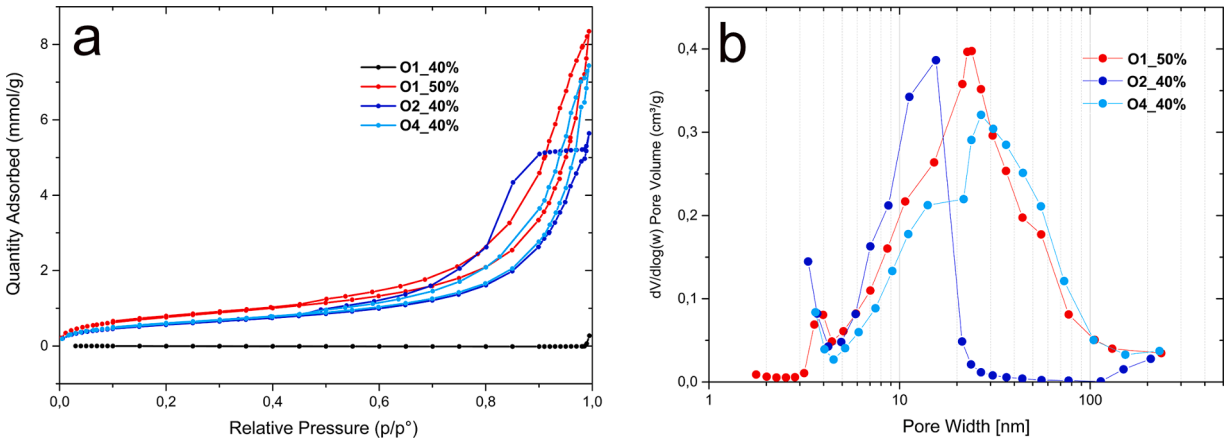

Fig. 4. a) Nitrogen adsorption and desorption isotherms of the porous SBE films. b) shows the BJH pore size distribution based on the desorption isotherm.

parameters lie relatively close to the monomer, with O1 being the most similar and O4 the furthest from the monomer. However, the polarity of O4 (δ_D) is the lowest, suggesting it is most compatible with the growing polymer chain. The oligomeric electrolyte content in the formulations was set at 40 wt% for all three oligomers. A formulation with 50 wt% O1 was also produced to investigate the effect of electrolyte content.

When cured, the SBE films all reached a high conversion, as confirmed through FTIR (Fig. 2). Here, the use of thermal curing is useful to achieve such a high conversion, since the viscosity of the resin is significantly decreased at higher temperature and vitrification effects on the curing can be avoided. The resulting SBEs turn opaque at various degrees, indicating that a phase separation has occurred to yield different morphologies (Fig. S4).

The oligomeric electrolyte could be fully extracted via solvent exchange and drying. Drying the films led to significant shrinkage which indicates that the polymer phase swells in the wet state (Fig. S5). The films shrunk 20–30% in volume upon removing the oligomeric electrolyte depending on which oligomer was used (see Table 2). The swelling was most pronounced in the case of O1, which can be explained by the fact that the smaller molecule more easily penetrates the pore walls and diffuses into the polymer phase. Consequently, the two phases cannot be considered completely decoupled, increasing the complexity of the system. Instead, it can best be described by a two-phase system containing a swollen porous polymer filled with a liquid electrolyte.

Microstructure

The microstructure of the dried films could be examined using FE-SEM. Micrographs of the cross sections can be seen in Fig. 3. Due to the significant shrinkage of the films upon drying, the true porosity is likely different. The swelling effect may lead to more narrow channels in reality. Conversely, due to the shrinkage, some pores may collapse and seem more closed than in the wet state. For this, more advanced studies would need to be performed to gain a better understanding of the true porosity. Nevertheless, comparisons between the formulations can be made. All formulations display a homogeneous distribution of pores at the micrometre size range (Fig. S6). At higher magnification, some differences can be noted. The structures seem to increase in size from O1 to O4 at 40 wt% electrolyte. A more open system can be seen in the O1 made with 50 wt% electrolyte compared to 40 wt%. However, altogether the structures look rather similar. A proper analysis of the morphology is limited by the resolution that was obtainable. Due to the roughness and porosity, increasing the magnification was challenging. Therefore, the pore size was quantified using nitrogen gas adsorption.

Fig. 4a shows the adsorption and desorption isotherms of the dried films. Surprisingly, O1_40% shows almost no porosity. This could be due to the presence of pores that are too narrow for analysis, or pores which close upon drying. It could also be a sign that a percolating phase separation is not fully achieved. Likely, a spinodal decomposition does not occur for this formulation. Similar behaviour has been seen previously for formulations with low porogen content [37]. Increasing the electrolyte content to 50 wt% leads to a drastic increase in adsorption, displaying an isotherm typical for mesoporous materials. The isotherms of O2 and O4 are also typical for mesoporous materials, displaying a hysteresis between the adsorption and desorption isotherm. O4_40% and O1_50% do not contain a plateau at high relative pressure, which suggests that they also contain macropores [38].

The pore size distribution (Fig. 4b) is rather broad for O4_40% and O1_50% over a range of 5–100 nm. O2_40% displays a narrower distribution at slightly lower pore size. The broad distribution could be due to the free radical-initiated chain growth mechanism which leads to a broad distribution of molecular weights and typically leads to a heterogeneous thermoset network and subsequently heterogeneous mesoporous morphology [39]. The average pore size lies at 10 nm compared to 14 nm for O4_40%. This suggests that the pore size increases with increasing chain length of the oligomeric porogen. There are several competing parameters which affect if and when a phase separation occurs, which can be explained by the Flory-Huggins equation (*Eq. (1)*) [13].

$$\Delta G \alpha RT\left(\frac{\phi_P}{P_P}\ln\phi_P + \phi_M \ln\phi_M + \frac{\phi_S}{P_S}\ln\phi_S + \sum \chi_{ij}\phi_i\phi_j\right) \quad (1)$$

ϕ_i and P_i is the volume fraction and degree of polymerization respectively of component P (polymer), M (monomer), and S (solvent). χ_{ij} is the interaction parameter based on the miscibility of the components. $\Delta G$is the free energy of mixing, which is below zero when the components are miscible. One driving force for phase separation is the increase in P_P, which will lead to less negative ΔG. Note that $\ln\phi_i$ will always be negative since $0 < \phi_i < 1$. Another driving force is the shift in the interaction parameter since it may differ between the polymer and monomer. When comparing O1-O4 at 40 wt%, the volume fractions can be considered similar. By changing the oligomeric porogen, two parameters compete, χ_{ij} and P_S. P_S increases with oligomer chain length, which leads to a less negative ΔG. This term seems to dominate in these systems, leading to phase separation at the largest size domains for the largest oligomers. This has been observed in several previous studies [20,40].

It is important to note that the Flory-Huggins equation does not perfectly describe our system. In particular, the heterogeneous increase of molecular weight in a free radical system leads to the formation of microgels which form prior to spinodal decomposition [39]. In this case, the elasticity of the network is an additional driving force leading to deswelling of the thermoset and subsequent phase separation [13]. Due to the high viscosity of O2 and particularly O4, such inhomogeneities are proposed to be more favoured.

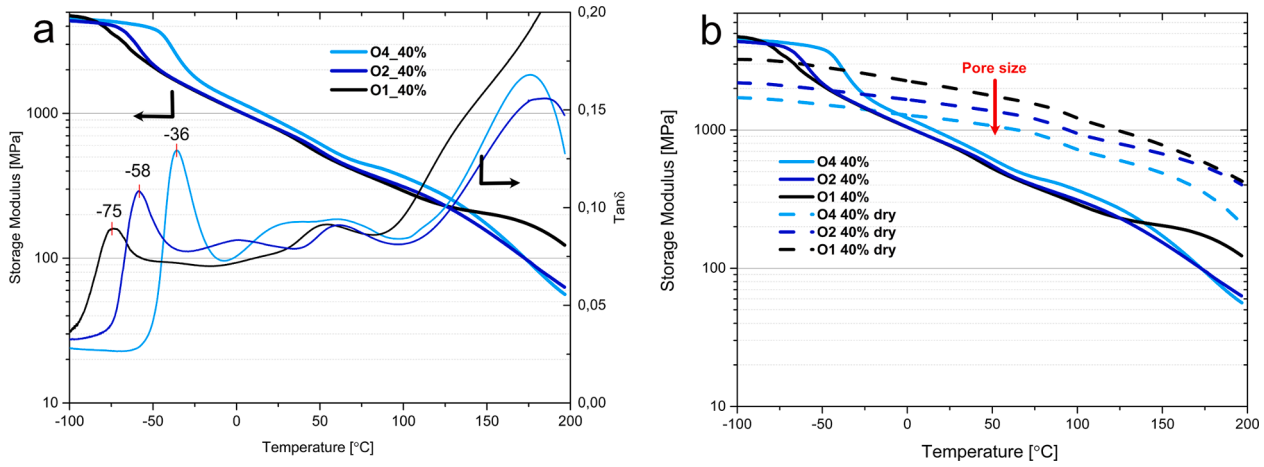

Fig. 5. a) Storage modulus and tan δ vs. temperature for wet SBEs (filled with oligomeric electrolyte) obtained from the DMA. b) Storage modulus vs. temperature for both wet and dried samples obtained from the DMA.

Table 3
Mechanical properties of SBE films obtained from DMA.

Sample		E', 25 °C [MPa]	Decrease in stiffness [%]
O4_40	Wet	850	−29
	Dry	1190	
O2_40	Wet	780	−52
	Dry	1520	
O1_40	Wet	770	−62
	Dry	2030	
O1_50	Wet	360	−68
	Dry	1110	

Thermomechanical properties

The thermomechanical behaviour of the formulations was examined both in the wet and dry state using DMA (Fig. 5). To gain insight into transitions in both phases, a broad temperature range was studied. In the wet samples, an initial transition is seen corresponding to the softening point of the oligomer. This ranges from −75 °C for O1 to −36 °C for O4. Thereafter, no clear transitions are seen below 150 °C, typical for highly crosslinked thermosets. A glass transition (T_g) of the thermoset can be seen at 174 °C for O4_40% and 183 °C for O2_40%. The T_g of the O1 formulations cannot be accurately determined due to evaporation of electrolyte, which hardens the polymer during the measurement, resulting in misleading data.

The storage modulus, measured via DMA, can give insight into the stiffness of the material (Table 3). The storage modulus at room temperature is the highest for O4_40% but in the same range for O2_40% and O1_40%. This trend is reversed when comparing the storage modulus of the dried samples (Fig. 4b). Here, the storage modulus of O1_40% is the highest and O4_40% is the lowest. This suggests that there are at least two competing effects: the pore size and solvent plasticization. In the dry state, O4_40% exhibits the largest pores and therefore the lowest storage modulus. However, due to the high viscosity and lower miscibility of O4, the plasticizing effect is limited and the storage modulus in the wet state only decreases by 29%. In contrast, O1_40% exhibits a high storage modulus in the dry state which is almost on par with the pure thermoset at room temperature (Fig. S7). This is further evidence of pore closure and the low porosity of O1_40% in the dry state. In the wet state, the plasticizing effect is significant, leading to a decrease in storage modulus by 62%. This trend is also well in line with the extent of shrinkage observed for the different samples. As expected, O1_50% exhibits a lower storage modulus than O1_40% due to the larger pores (Fig. S8). A similar plasticizing effect is also observed for O1_50%. Altogether, this shows the need to take both these effects into account when developing SBEs. Increasing the pore size will lead to losses in mechanical stiffness. On the other hand, an increasing pore size facilitates ion transport. Likewise, using an electrolyte with a low viscosity and higher miscibility as a porogen may soften the polymer network. However, a low viscosity is often synonymous with a high ionic conductivity.

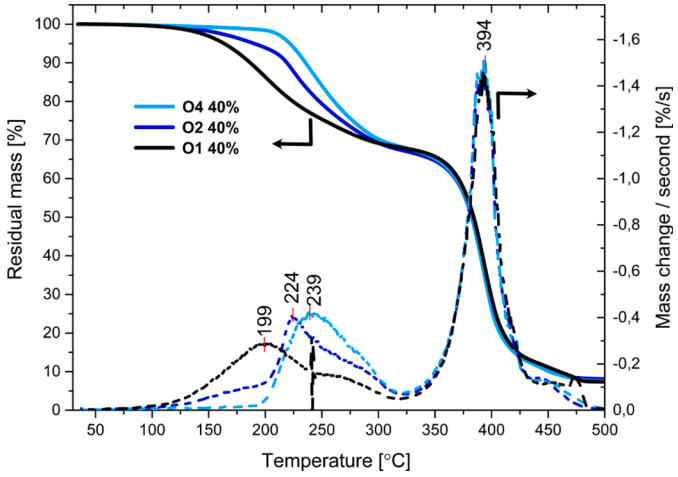

Fig. 6. Residual mass and mass change vs. temperature, obtained from TGA.

The thermal stability of the SBEs was evaluated using TGA. Fig. 6 clearly shows that the liquid phase starts to evaporate at different temperatures depending on the length of the oligomer. For O4, the mass loss starts to occur at high temperatures where PTMC-based electrolytes star to degrade, suggesting the volatility is very low [36]. In general, the evaporation occurs slowly due to the liquids being restricted to the pores, leading to a broad mass loss derivative peak. The polymer phase starts to break down at the same temperature for all formulations, showing that the thermosets are chemically similar. Finally, the 10 wt% left at 500 °C corresponds to residuals from LiTFSI and the thermoset. In general, the thermal stabilities of these SBEs lie in-between fully solid-state polymer electrolytes and liquid electrolytes. The thermal stability is greatly improved in comparison to commercial liquid electrolytes based on EC/DMC and EC/DEC where in particular the linear carbonate evaporates rapidly at low temperatures. [41,42]

Ionic conductivity

The temperature dependence of the ion conductivity for the different SBE films can be seen in Fig. 7a. To obtain the conductivity values, EIS measurements were run on SBE films (100 μm) sandwiched between two

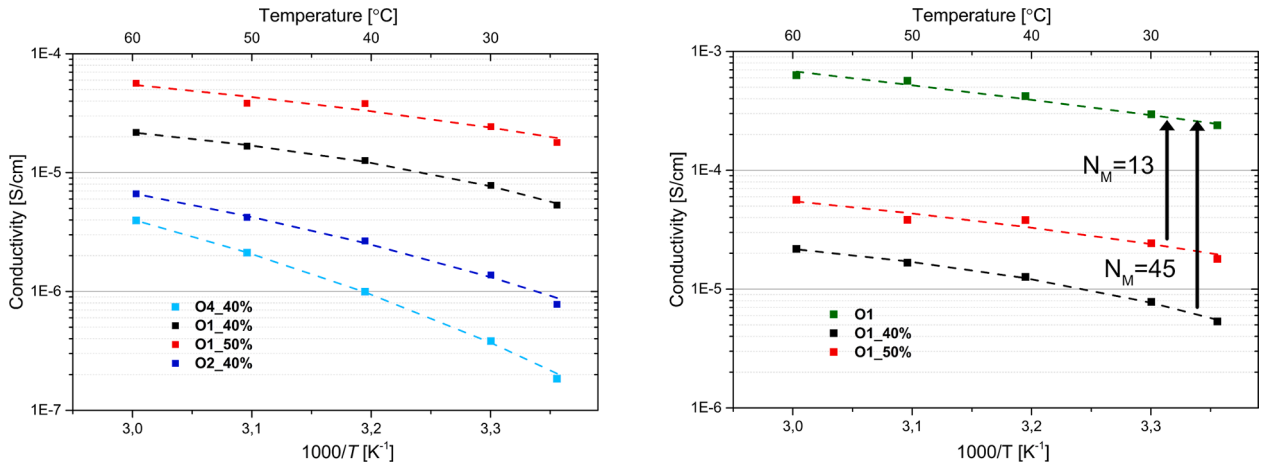

Fig. 7. Temperature dependence of ion conductivity for a) all SBE samples and b) O1 SBEs and pure O1 electrolyte. Dashed lines refer to the VFT fits that have been applied to the data.

stainless steel electrodes. Equivalent circuits were applied similar to the ones used by Sångeland et al. to model EIS data from double layer polymer electrolytes. [43] In all cases, two resistances could be identified. A first resistance (R_{liq}) was identified to be associated with the oligomeric carbonate electrolyte, and the second resistance (R_i) as an interfacial resistance. For O4_40% and O2_40%, an equivalent circuit seen in Fig. S9 was applied. For the O1 samples (O1_40% and O1_50%), a simpler circuit could be applied, seen in Fig. S10. The effective ionic conductivity was obtained from the sum of R_{liq} and R_i.

Owing to the higher ionic conductivity of pure O1, the SBEs also display a superior conductivity. This does however not tell the full story. A useful measure when comparing the SBEs, is the MacMullin number (N_M), which is often used to evaluate separators. [44]

$$N_M = \frac{\sigma_l}{\sigma_{eff}} \quad (2)$$

Here σ_l is the pure liquid electrolyte conductivity and σ_{eff} is the effective conductivity through the separator, in this case the SBE. N_M decreases drastically from 45 to 13 between O1_40% and O1_50%, as seen in Fig. 7b. This is partly due to the additional 10 wt% oligomeric electrolytes, but can also be assigned to the large pore size in the porous polymer. N_M is 34 for O2_40% and 22 for O4_40%, also correlating well with the pore size. O1_50% has half the N_M that O4_40% has, despite having similar average pore size. This indicates that the size of the oligomeric molecule also plays a role. O4 is more restricted than O1 by pores that are the same size. Interestingly, the N_M of O1_50% is also similar to that of several commercial separators [44].

VFT fits were applied for all SBEs (dashed lines in Fig. 7) and show a rather good agreement. The temperature dependence of the ion conduction in the SBEs is similar to the temperature dependence of the respective oligomers used. This suggests that ion conduction mainly occurred in the oligomer phase, and that the porous thermoset mainly increased the tortuosity i.e. resulted in longer ionic pathways through the small pores (<100 nm).

4. Conclusions

In this study, three linear carbonates with varying chain lengths were used as porogens and ion conductors in SBEs. This was done to explore the realm between a liquid-containing SBE and a polymer blend containing two polymer phases, as well as to improve the thermal stability of the SBEs. By changing the oligomer chain length, the PIPS process was changed, even when using the same monomer. Larger pores were achieved when increasing the oligomer chain length and increasing the electrolyte content. The complex interplay of the phases and how this affects the mechanical properties were described. The pore size clearly has an effect on the mechanical stiffness of the SBE. However, the oligomers also plasticise the polymer phase to different extents, which needs to be considered when developing the SBE. The thermal stability was also significantly enhanced by increasing the oligomer chain length by a few repeating units compared to commercially used solvents. When quantifying the ion conduction of the SBEs, N_M was shown to be a useful tool to validate the tortuosity of the SBEs, where a low N_M correlated well with a large pore size. Although several properties improved when using longer carbonates (O2 and O4), the inherently low conductivities of these carbonates limit their electrochemical performance. However, using an oligomer with a higher intrinsic ionic conductivity would allow for higher molecular weights which consequently could be a promising route for achieving a higher thermal and mechanical performance as well as a lower N_M.

Declaration of Competing Interest

The authors declare that they have no known competing financial interests or personal relationships that could have appeared to influence the work reported in this paper.

Data availability

Data will be made available on request.

Acknowledgements

The authors gratefully acknowledge financial support from BASE Battery Sweden (Vinnova grant: 2019–00064), STandUP for Energy, and ECO^{2}LIB (European Union H2020 research and innovation programme under Grant agreement No 875514).

The research group Kombatt at Chalmers and KTH is acknowledges for the collaboration around structural batteries.

Supplementary materials

Supplementary material associated with this article can be found, in the online version, at doi:10.1016/j.electacta.2023.142176.

References

[1] IPCC, Climate Change 2022: mitigation of Climate Change. Contribution of Working Group III to the Sixth Assessment Report of the Intergovernmental Panel

On Climate Change, Cambridge University Press, Cambridge, UK and New York, NY, USA, 2022.
[2] J. Kalhoff, G.G. Eshetu, D. Bresser, S. Passerini, Safer electrolytes for lithium-ion batteries: state of the art and perspectives, ChemSusChem 8 (13) (2015) 2154–2175, https://doi.org/10.1002/cssc.201500284.
[3] L.E. Asp, M. Johansson, G. Lindbergh, J. Xu, D. Zenkert, Structural battery composites: a review, Funct. Compos. Struct. 1 (4) (2019), 042001, https://doi.org/10.1088/2631-6331/ab5571.
[4] D. Zhou, D. Shanmukaraj, A. Tkacheva, M. Armand, G.X. Wang, Polymer electrolytes for lithium-based batteries: advances and prospects," (in English), Chem-Us 5 (9) (Sep 12 2019) 2326–2352, https://doi.org/10.1016/j.chempr.2019.05.009.
[5] C. Heubner, et al., From lithium-metal toward anode-free solid-state batteries: current developments, issues, and challenges, Adv. Funct. Mater. 31 (51) (2021), 2106608, https://doi.org/10.1002/adfm.202106608.
[6] A. Pei, G. Zheng, F. Shi, Y. Li, Y. Cui, Nanoscale nucleation and growth of electrodeposited lithium metal, Nano Lett. 17 (2) (2017) 1132–1139, https://doi.org/10.1021/acs.nanolett.6b04755.
[7] F. Peters, et al., Correlation of mechanical and electrical behavior of polyethylene oxide-based solid electrolytes for all-solid state lithium-ion batteries, Batteries 5 (1) (2019) 26, https://doi.org/10.3390/batteries5010026.
[8] M. Willgert, M.H. Kjell, E. Jacques, M. Behm, G. Lindbergh, M. Johansson, Photoinduced free radical polymerization of thermoset lithium battery electrolytes, Eur. Polym. J. 47 (12) (2011) 2372–2378, https://doi.org/10.1016/j.eurpolymj.2011.09.018. /12/01/2011.
[9] R. Andersson, G. Hernández, J. See, T.D. Flaim, D. Brandell, J. Mindemark, Designing polyurethane solid polymer electrolytes for high-temperature lithium metal batteries, ACS Appl. Energy Mater. 5 (1) (2022) 407–418, https://doi.org/10.1021/acsaem.1c02942.
[10] E. Wetzel, Reducing weight: multifunctional composites integrate power, communications and structures, AMPTIAC Q. 8 (4) (2004) 91–95.
[11] J.F. Snyder, R.H. Carter, E.D. Wetzel, Electrochemical and mechanical behavior in mechanically robust solid polymer electrolytes for use in multifunctional structural batteries, Chem. Mater. 19 (15) (2007) 3793–3801, https://doi.org/10.1021/cm070213o.
[12] P.-A.T. Nguyen, J. Snyder, Multifunctional properties of structural gel electrolytes, ECS Trans. 11 (32) (2008) 73–83, https://doi.org/10.1149/1.2992495.
[13] H.M.J. Boots, J.G. Kloosterboer, C. Serbutoviez, F.J. Touwslager, Polymerization-induced phase separation. 1. conversion−phase diagrams, Macromolecules 29 (24) (1996) 7683–7689, https://doi.org/10.1021/ma960292h.
[14] S. Eeltink, F. Svec, Recent advances in the control of morphology and surface chemistry of porous polymer-based monolithic stationary phases and their application in CEC, Electrophoresis 28 (1–2) (2007) 137–147, https://doi.org/10.1002/elps.200600573.
[15] M.H. Mohamed, L.D. Wilson, Porous copolymer resins: tuning pore structure and surface area with non reactive porogens, Nanomaterials 2 (2) (2012) 163–186, https://doi.org/10.3390/nano2020163.
[16] B.A. Hermawan, Mutakin, A.N. Hasanah, Role of porogenic solvent type on the performance of a monolithic imprinted column, Chem. Pap. 75 (4) (2021) 1301–1311, https://doi.org/10.1007/s11696-020-01399-5.
[17] F.S. Macintyre, D.C. Sherrington, Control of porous morphology in suspension polymerized poly(divinylbenzene) resins using oligomeric porogens, Macromolecules 37 (20) (2004) 7628–7636, https://doi.org/10.1021/ma0491053.
[18] C. Viklund, F. Svec, J.M.J. Fréchet, K. Irgum, Monolithic, “molded”, porous materials with high flow characteristics for separations, catalysis, or solid-phase chemistry: control of porous properties during polymerization, Chem. Mater. 8 (3) (1996) 744–750, https://doi.org/10.1021/cm950437j.
[19] J. Wang, S. Shen, X. Lu, F. Ye, One-pot preparation of an organic polymer monolith by thiol-ene click chemistry for capillary electrochromatography, J. Sep. Sci. 40 (15) (2017) 3144–3152, https://doi.org/10.1002/jssc.201700110.
[20] M.W. Schulze, M.A. Hillmyer, Tuning mesoporosity in cross-linked nanostructured thermosets via polymerization-induced microphase separation, Macromolecules 50 (3) (2017) 997–1007, https://doi.org/10.1021/acs.macromol.6b02570.
[21] G. Hasegawa, K. Kanamori, K. Nakanishi, S. Yamago, Fabrication of highly crosslinked methacrylate-based polymer monoliths with well-defined macropores via living radical polymerization, Polymer (Guildf.) 52 (21) (2011) 4644–4647, https://doi.org/10.1016/j.polymer.2011.08.028.
[22] F.R. Mansour, S. Waheed, B. Paull, F. Maya, Porogens and porogen selection in the preparation of porous polymer monoliths, J. Sep. Sci. 43 (1) (2020) 56–69, https://doi.org/10.1002/jssc.201900876.
[23] S.A. Chopade, J.G. Au, Z. Li, P.W. Schmidt, M.A. Hillmyer, T.P. Lodge, Robust polymer electrolyte membranes with high ambient-temperature lithium-ion conductivity via polymerization-induced microphase separation, ACS Appl. Mater. Interfaces (2017), https://doi.org/10.1021/acsami.7b02514.
[24] M.W. Schulze, L.D. McIntosh, M.A. Hillmyer, T.P. Lodge, High-modulus, high-conductivity nanostructured polymer electrolyte membranes via polymerization-induced phase separation, Nano Lett. 14 (1) (2014) 122–126, https://doi.org/10.1021/nl4034818.
[25] N. Shirshova, et al., Structural supercapacitor electrolytes based on bicontinuous ionic liquid–epoxy resin systems, J. Mater. Chem. 1 (48) (2013) 15300, https://doi.org/10.1039/c3ta13163g.
[26] N. Shirshova, et al., Composition as a means to control morphology and properties of epoxy based dual-phase structural electrolytes, J. Phys. Chem. C 118 (49) (2014) 28377–28387, https://doi.org/10.1021/jp507952b.
[27] S.J. Kwon, T. Kim, B.M. Jung, S.B. Lee, U.H. Choi, Multifunctional epoxy-based solid polymer electrolytes for solid-state supercapacitors, ACS Appl. Mater. Interfaces 10 (41) (2018) 35108–35117, https://doi.org/10.1021/acsami.8b11016.
[28] Y.H. Song, T. Kim, U.H. Choi, Tuning morphology and properties of epoxy-based solid-state polymer electrolytes by molecular interaction for flexible all-solid-state supercapacitors, Chem. Mater. 32 (9) (2020) 3879–3892, https://doi.org/10.1021/acs.chemmater.0c00041.
[29] E.B. Gienger, P.-A.T. Nguyen, W. Chin, K.D. Behler, J.F. Snyder, E.D. Wetzel, Microstructure and multifunctional properties of liquid + polymer bicomponent structural electrolytes: epoxy gels and porous monoliths, J. Appl. Polym. Sci. 132 (42) (2015), https://doi.org/10.1002/app.42681.
[30] Q. Feng, et al., The ionic conductivity, mechanical performance and morphology of two-phase structural electrolytes based on polyethylene glycol, epoxy resin and nano-silica, Mater. Sci. Eng. B Solid State Mater. Adv. Technol. 219 (2017) 37–44, https://doi.org/10.1016/j.mseb.2017.03.001. /05/01/2017.
[31] A.J. Manly, W.E. Tenhaeff, One-step fabrication of robust lithium ion battery separators by polymerization-induced phase separation, J. Mater. Chem. 10 (19) (2022) 10557–10568, https://doi.org/10.1039/d1ta10730e.
[32] N. Ihrner, W. Johannisson, F. Sieland, D. Zenkert, M. Johansson, Structural lithium ion battery electrolytes via reaction induced phase-separation," (in English), J. Mater. Chem. 5 (48) (Dec 28 2017) 25652–25659, https://doi.org/10.1039/c7ta04684g.
[33] L.E. Asp, et al., A structural battery and its multifunctional performance, Adv. Energy Sustainability Res. p. 2000093 (2021), https://doi.org/10.1002/aesr.202000093.
[34] L.M. Schneider, N. Ihrner, D. Zenkert, M. Johansson, Bicontinuous electrolytes via thermally initiated polymerization for structural lithium ion batteries, ACS Appl. Energy Mater. 2 (6) (2019) 4362–4369, https://doi.org/10.1021/acsaem.9b00563.
[35] J. Mindemark, S. Tang, H. Li, L. Edman, Ion transport beyond the polyether paradigm: introducing oligocarbonate ion transporters for efficient light-emitting electrochemical cells, Adv. Funct. Mater. 28 (32) (2018), 1801295, https://doi.org/10.1002/adfm.201801295.
[36] B. Sun, J. Mindemark, K. Edström, D. Brandell, Polycarbonate-based solid polymer electrolytes for Li-ion batteries, Solid State Ionics 262 (2014) 738–742, https://doi.org/10.1016/j.ssi.2013.08.014.
[37] R. Kurt, L. Simon, R. Penterman, E. Peeters, H. De Koning, D.J. Broer, Control over the morphology of porous polymeric membranes for flow through biosensors, J. Memb. Sci. 321 (1) (2008) 51–60, https://doi.org/10.1016/j.memsci.2007.12.020.
[38] K.S.W. Sing, Reporting physisorption data for gas/solid systems with special reference to the determination of surface area and porosity (Recommendations 1984), Pure Appl. Chem. 57 (4) (1985) 603–619, https://doi.org/10.1351/pac198557040603.
[39] K. Kanamori, J. Hasegawa, K. Nakanishi, T. Hanada, Facile synthesis of macroporous cross-linked methacrylate gels by atom transfer radical polymerization, Macromolecules 41 (19) (2008) 7186–7193, https://doi.org/10.1021/ma800563p.
[40] J. Hasegawa, K. Kanamori, K. Nakanishi, T. Hanada, S. Yamago, Pore formation in poly(divinylbenzene) networks derived from organotellurium-mediated living radical polymerization, Macromolecules 42 (4) (2009) 1270–1277, https://doi.org/10.1021/ma802343a.
[41] V. Nilsson, A. Kotronia, M. Lacey, K. Edström, P. Johansson, Highly concentrated LiTFSI–EC electrolytes for lithium metal batteries, ACS Appl. Energy Mater. 3 (1) (2020) 200–207, https://doi.org/10.1021/acsaem.9b01203.
[42] D.W. McOwen, D.M. Seo, O. Borodin, J. Vatamanu, P.D. Boyle, W.A. Henderson, Concentrated electrolytes: decrypting electrolyte properties and reassessing Al corrosion mechanisms, Energy Environ. Sci. 7 (1) (2014) 416–426, https://doi.org/10.1039/c3ee42351d.
[43] C. Sångeland, T. Tjessem, J. Mindemark, D. Brandell, Overcoming the obstacle of polymer–polymer resistances in double layer solid polymer electrolytes, J. Phys. Chem. Lett. 12 (11) (2021) 2809–2814, https://doi.org/10.1021/acs.jpclett.1c00366.
[44] J. Landesfeind, J. Hattendorff, A. Ehrl, W.A. Wall, H.A. Gasteiger, Tortuosity determination of battery electrodes and separators by impedance spectroscopy, J. Electrochem. Soc. 163 (7) (2016) A1373–A1387, https://doi.org/10.1149/2.1141607jes.